NASA TECHNICAL NOTE

NASA TN D-6587

SOME CHARACTERISTICS OF TURBULENT BOUNDARY LAYERS IN RAPIDLY ACCELERATED FLOWS

by Paul F. Brinich and Harvey E. Neumann

Lewis Research Center
Cleveland, Ohio 44135

NATIONAL AERONAUTICS AND SPACE ADMINISTRATION • WASHINGTON, D. C. • DECEMBER 1971

1. Report No.	2. Government Accession No.	3. Recipient's Catalog No.
NASA TN D-6587		

4. Title and Subtitle	5. Report Date
SOME CHARACTERISTICS OF TURBULENT BOUNDARY LAYERS IN RAPIDLY ACCELERATED FLOWS	December 1971
	6. Performing Organization Code
7. Author(s)	8. Performing Organization Report No.
Paul F. Brinich and Harvey E. Neumann	E-6496
	10. Work Unit No.
9. Performing Organization Name and Address	132-15
Lewis Research Center National Aeronautics and Space Administration Cleveland, Ohio 44135	11. Contract or Grant No.
	13. Type of Report and Period Covered
12. Sponsoring Agency Name and Address	Technical Note
National Aeronautics and Space Administration Washington, D.C. 20546	14. Sponsoring Agency Code

15. Supplementary Notes

16. Abstract

An analysis of time - mean-turbulent-boundary-layer velocity profiles measured in a rapidly accelerating flow suggests that the outer region of the velocity profiles consists of essentially inviscid, rotational flow. The extent of this inviscid outer region was observed in some cases to exceed 90 percent of what is ordinarily thought of as the turbulent-boundary-layer thickness. On the other hand, the inner frictional region of these velocity profiles appears to have turbulent characteristics similar to those of more conventional turbulent boundary layers. Hence, the outer edge boundary condition for this inner region is more properly the external rotational flow region than the free stream.

17. Key Words (Suggested by Author(s))

Fluid mechanics
Turbulent boundary layers
Accelerated flow
Entrainment

18. Distribution Statement

Unclassified - unlimited

19. Security Classif. (of this report)	20. Security Classif. (of this page)	21. No. of Pages	22. Price*
Unclassified	Unclassified	31	$3.00

* For sale by the National Technical Information Service, Springfield, Virginia 22151

SOME CHARACTERISTICS OF TURBULENT BOUNDARY LAYERS IN RAPIDLY ACCELERATED FLOWS

by Paul F. Brinich and Harvey E. Neumann

Lewis Research Center

SUMMARY

An analysis of time - mean-turbulent-boundary-layer-velocity profiles measured in a rapidly accelerating flow suggests that the outer region of the velocity profiles consists of essentially inviscid, rotational flow. The extent of this inviscid outer region was observed in some cases to exceed 90 percent of what is ordinarily thought of as the turbulent-boundary-layer thickness. On the other hand, the inner frictional region of these velocity profiles appears to have turbulent characteristics similar to those of more conventional turbulent boundary layers. Hence, the outer edge boundary condition for this inner region is more properly the external rotational flow region than the free stream.

INTRODUCTION

The development of the turbulent boundary layer in a strong favorable pressure gradient has generated an unusual amount of interest among aerodynamicists during the past few years. This interest has resulted from the inability of certain computing techniques to predict accurately turbulent-boundary-layer development and heat transfer in rapidly accelerating flows through nozzles as well as from the appearance of laminarization of the turbulent boundary layer during rapid acceleration. As evidence for the anomalous behavior of the turbulent boundary layer and the occurrence of laminarization, use is frequently made of heat-transfer data which in general show reductions in heat-transfer level compared to accepted computational methods (ref. 1). Occasionally boundary-layer profiles are provided in these investigations, but usually they are few in number and on a scale too small to give much detail. The intent of this investigation was therefore to obtain mean velocity profiles of a rapidly accelerating turbulent boundary layer having sufficient thickness to facilitate accurate profile measurement and a sufficient number of

survey stations to study the profile development in a streamwise direction. No heat transfer or turbulence measurements were made.

Some of the velocity profiles to be presented in this report and the method of analyzing them have already been presented in reference 2, where it was concluded that for this experiment entrainment of the free stream into the turbulent boundary layer ceases when the acceleration becomes large. Also, it was later suggested in reference 3 that for incompressible flow the criterion for negative entrainment is

$$2(\delta^* + \theta)\frac{d \ln u_\infty}{dx} > c_f$$

where δ^* is the boundary-layer displacement thickness, δ is the boundary-layer momentum thickness, u_∞ is the free-stream velocity, x is the axial distance from the beginning of the test section, and c_f is the local friction coefficient. This equation indicates the importance of a sufficiently thick boundary layer as well as the need for a large acceleration.

SYMBOLS

c_f local friction coefficient

K pressure-gradient parameter, $(\nu_\infty/U_\infty^2)(d\, u_\infty/dx)$

P_0 stagnation pressure in plenum

p static pressure

R radius of curvature of channel wall

u velocity

u_τ shear velocity

x axial distance from beginning of test section

y distance measured perpendicular to wall

y^+ wall distance parameter, $u_\tau y/\nu$

δ boundary-layer velocity thickness at $u/u_\infty = 0.99$

δ^* boundary-layer displacement thickness, $\displaystyle\int_0^\delta \left(1 - \frac{\rho u}{\rho_\infty u_\infty}\right) dy$

θ boundary-layer momentum thickness, $\int_0^{\delta} \frac{\rho u}{\rho_\infty u_\infty}\left(1 - \frac{u}{u_\infty}\right)dy$

ν kinematic viscosity

ρ density

Subscripts:

W wall conditions

∞ free-stream conditions

APPARATUS AND PROCEDURE

The test facility in which the present experiment was conducted is the 4- by 10-inch wind tunnel shown in figure 1. Processed dry air at atmospheric pressure, a temperature of 24° C (75° F), and a dew point -29° C (-20° F) was supplied to the plenum from whence it flowed through the tunnel, diffuser, and exhaust system, which was maintained at a pressure of 1.0 to 2.7×10^4 newtons per square meter (3 to 8 in. of mercury absolute). The test section in which the favorable pressure gradient was generated is indicated in the center of the tunnel in figure 1. The pertinent dimensions and shape of the region where measurements were made are shown on the upper part of figure 2. Since the test section was operated with sonic flow at the minimum point and supersonic flow downstream, and since no attempt was made to disperse the compression waves in the supersonic region, a strong oblique shock was generated on the curved wall about 7.6 centimeters (3 in.) downstream of the throat. Hence, quantitative flow measurements were made only up to this point, the shock - boundary-layer interaction being of no immediate interest. A 91-centimeter (36-in.) length of flat wall preceded the test section and was blended into a rectangular bellmouth in the plenum. Likewise, a similar length of flat wall lead to the diffuser, which had an opening 25.4 centimeters (10 in.) high.

The test section was machined of heavy aluminum weldments and finished to a root-mean-square surface smoothness of about 0.41 micrometer (16 μin.) as were also the flat-wall extensions upstream and downstream of the test section. The side walls were thick plate glass extending over the entire tunnel length and were used for visualization purposes. Static-pressure orifices and holes for introducing boundary-layer probes were provided on the flat and contoured walls along the centerline at 2.54-centimeter (1-in.) intervals. All the probe holes had smooth fitting plugs and were sealed against air leakage. Probe holes on both the flat and curved walls were drilled so that the tip of the probe traversed the flow in a straight line perpendicular to the wall, starting at the

point of contact. Thus, the probing plane was always perpendicular to the axial direction (x-axis) for the flat wall, although this was not always true for the curved wall.

A sketch of the pitot probe used to survey the boundary layer and the method of installation is shown in figure 3 for the flat wall. The probe tip was fabricated of 0.071-centimeter- (0.028-in. -) outside-diameter by 0.015-centimeter- (0.006-in. -) thick wall tubing, the end of which was flattened and lapped to an external height of 0.015 centimeter (0.006 in.) with a 0.005-centimeter- (0.002-in. -) thick wall. The probe position was adjusted manually with a fine-pitch screw feed device, and the probe wall contact was established electrically with a sensitive ohmmeter. The probe position relative to the wall was measured with 5.08-centimeter (2-in.) stroke machinist's dial indicator to an accuracy of 0.0012 centimeter (0.0005 in.). Pressures were measured with mercury and tetracbromoethylene manometers and with transducers to an accuracy of ±69 newtons per square meter (±0.01 psi).

In making the boundary-layer surveys it was necessary, from the standpoint of convenience and because of space limitations, to probe through the top wall of the tunnel only. Hence, to measure the boundary-layer profiles on the flat wall, the upper contoured and lower flat test section walls shown in figures 1 and 2 were interchanged.

In order to determine to what extent the boundary-layer flow departed from the desired two-dimensional form, the flow direction at the wall was examined in the following manner. A sheet of plain white plastic sheeting having a pressure-sensitive backing (commonly known as contact paper) was attached to each wall where it was desired to check the angularity of the flow. A mixture of lamp black paint coloring thinned with boiled linseed oil was used to place small dots on the sheeting at regular intervals. When the airflow was turned on, these small dots would stream in the direction of the flow and give a clear indication of any flow angularity. After the traces had developed sufficiently (usually a minute or so), the flow was shut off and the traces were allowed to air dry (several hours). The plastic sheeting was then removed from the walls so that it could be conveniently examined or photographed.

Velocity profiles were computed from the measured pitot pressures (corrected for normal shock when the flow became supersonic) and the adjacent wall static pressure, which was assumed constant normal to the wall, except where noted. The total temperature of the flow was assumed constant everywhere, and the aerodynamic center of the pitot tube was considered to coincide with the geometric center. Velocity measurements, based on accuracy of pressure measurements, are believed to be accurate within ±0.5 percent, with any wall interference effects of the probe approaching the wall neglected.

RESULTS AND DISCUSSION

Pressure Distribution

The static- to total-pressure ratio along the flat and curved walls is indicated in figure 2. It can be noted that the pressure distribution is favorable all along the flat wall, whereas on the curved wall it is initially unfavorable but then declines rapidly. The decrease in pressure along the curved wall is so rapid that the point where sonic velocity occurs is more than 2.54 centimeters (1 in.) upstream of the geometric throat, whereas on the flat wall the sonic point occurs about 2.54 centimeters (1 in.) downstream of the throat. Such pressure distributions for the flat and curved walls are expected from potential flow considerations.

The contrast between the pressure distributions is illustrated also in figure 4, where a pressure gradient parameter K defined by

$$K = \frac{\nu_\infty}{u_\infty^2} \frac{du_\infty}{dx}$$

is plotted. This parameter has been used by various investigators, for example, the authors of reference 4, as a criterion for the appearance of flow laminarization when the stream is initially turbulent. A value of K of about 3×10^{-6} is generally taken as the lower limit at which laminarization can occur. According to figure 4, only 1/10 of this value was reached on the flat wall and 1/3 on the curved. Hence, laminarization is certainly out of the question on the flat wall and probably not too important on the curved. This, of course, should not be taken to mean that laminarization occurs suddenly or that the profiles have not been markedly distorted by the velocity gradient.

Flow Visualization

The possibility of analyzing the boundary-layer flow quantitatively in the present tests depends to a large extent on how two-dimensional the flow actually is. An examination of the traces obtained on the curved and flat walls in figure 5 indicates a fairly rectilinear flow along the flat wall with appreciable secondary flows starting in the region of concave curvature along the contoured wall. Another characteristic is the uniformly increasing trace lengths on the flat wall as the flow accelerates in distinction to the shortening trace lengths on the curved wall in the neighborhood of the adverse pressure gradient. The shortening of the traces is indicative of a reduction in wall shear caused by the static-pressure increase. The secondary flows indicated by the diverging traces

start at $x = 15$ centimeters (6 in.), which is the point where the concave curvature begins. These secondary flows are caused by an unstable condition in the turbulent boundary layer whereby those parts of the boundary layer near the free stream, which have a relatively large momentum, displace the low-momentum flow near the wall, because of centrifugal forces. The low-momentum fluid near the wall is squeezed out laterally and makes its way onto the tunnel sidewalls, where it continues to flow downstream in the form of a corner vortex. This continues until the wall curvature reverses sign and the static pressure begins to decrease, at which point a vortex of the opposite sense begins to form and tends to cancel the original secondary flow.

Flow instabilities such as those just discussed make it almost impossible to make an accurate analysis of the boundary layer along a concave wall. This will become evident in the next section, where profiles obtained on both walls will be described.

Boundary-Layer Profiles

The term "boundary layer" in general aerodynamic usage refers to the velocity distribution in the neighborhood of a solid surface in contact with a flowing stream as a result of viscous forces, whether laminar or turbulent. In actual practice it is not always easy to distinguish whether such a distribution is the immediate consequence of viscous forces, potential flow velocity variations, or unusual vorticity distributions, resulting, for example, from wakes, curved shock waves, etc. As a result, the terms "boundary layer" and "velocity profile" will be used interchangeably, and the term "frictional boundary layer" will be reserved for those velocity profiles or parts thereof which are a direct consequence of local viscous forces, laminar and/or turbulent.

Boundary-layer profiles for the flat and the contoured wall are presented in figures 6 and 7 as the ratio of local to free-stream velocity u/u_∞ plotted against the logarithm of the distance from the wall y. The semilog presentation was used because it magnified the regions near the wall where the boundary-layer velocity was changing rapidly and because it indicated whether the profiles had the straight-line variation commonly associated with the "law of the wall."

The flat-wall profiles in figure 6 for $x = 0$ and 5.1 centimeters (0 and 2 in.) are conventional appearing turbulent velocity profiles having a linear "law of the wall" region that extends out to about $y = 0.127$ centimeter (0.05 in.), followed by a "wake" region extending to the free stream. The approximate regions are indicated in figure 6; a dashed line forms an outward extension of the "law of the wall" region. The points nearest the wall ($y = 0.0076$ cm or 0.003 in.) are probably very close to the edge of the laminar sublayer, based on a value of $y^+ = 30$ and an assumed friction coefficient of 0.003. In progressing downstream, the inner part of the velocity profile rises relative to the outer wake, and at $x = 20.3$ centimeters (8 in.) the entire profile can be

approximated by a single straight line out to the free stream. This is similar in appearance to a fully developed pipe profile, except that in the present instance the profile occurs in an accelerating flow rather than in a constant-velocity flow. Beyond $x = 20.3$ centimeters (8 in.) the inner part of the profile continues to rise, with a more gradual return to the free-stream velocity at the outer edge. One of the most striking features of figure 6 concerns the relative abruptness with which the more conventional turbulent boundary layer ($x \leq 15$ cm or 6 in.) approaches the free stream compared to the long gradual tailing off of the accelerated boundary layer. This makes a dubious matter of determining a boundary-layer thickness and the proper edge conditions for a strongly accelerated profile.

In contrast to the flat wall, the curved wall shows a markedly different and disorderly boundary-layer development, as indicated in figure 7. This is particularly true up to about $x = 20.3$ centimeters (8 in.), in which region there exist strong destabilizing forces and secondary flows caused by the concave curvature of the walls and the adverse pressure gradient. The markedly different behavior of the profiles at $x = 15$ centimeters (6 in.) in figures 6 and 7 is to be noted, even though both profiles were obtained before any wall curvature took place. At $x = 23$ centimeters (9 in.) the concave curvature has ceased and the profile development takes place in a more orderly fashion, but with large regions of small velocity gradient for $y > 0.08$ centimeter (0.03 in.) and extremely large gradients near the wall. The profile at $x = 23$ centimeters (9 in.) occurs at the point where the pressure gradient parameter K reached a maximum value of 1.28×10^{-6}. Downstream of this point, as the pressure gradient parameter diminishes, the profiles again acquire the straight-line "law of the wall" variation. This was also true of profiles at $x = 33.0$ and 35.6 centimeters (13 and 14 in.), which are not shown in figure 7 because it was not possible to define a free-stream velocity u_∞. It should be noted here that all the profiles shown in figures 6 and 7 were nondimensionalized with a free-stream velocity u_∞ which remained constant for at least 1.27 centimeters (0.5 in.) and very often was constant for 3.8 centimeters (1.5 in.) (as determined from a constant value of the total pressure). The profiles at $x = 33.0$ and 35.6 centimeters (13 and 14 in.) had total-pressure profiles which continued to rise at the limit of the probe travel of 5.08 centimeters (2 in.) and showed no tendency to level off. Such behavior is explainable by probe angle of attack effects and a variation of the free-stream static pressure.

Except for the initial profiles at $x = 0$ and 5.1 centimeters (0 and 2 in.), the flat- and curved-wall profiles differ considerably in their development. The curved-wall profiles experience a strong deceleration near the wall in the region of concave wall curvature, a static-pressure variation normal to the wall, and a wall curvature instability, all of which make it very difficult to analyze the profiles. In the region of convex curvature the turning instability vanished, and an attempt was made to assess the importance of the static-pressure variation normal to the wall. This was done by assuming that the

streamline curvature in the boundary layer over the convexly curved surface was concentric with the surface. The static pressure $p(\xi)$ at any distance ξ normal to the surface was then given by

$$p(\xi) = p_w + \int_0^{\xi} \frac{\rho u^2}{R + y} dy$$

where p_w is the measured wall value, and the integral is the contribution of the centrifugal force. This static-pressure variation and the experimentally measured total-pressure variation was used to define implicitly the velocity variation. However, because of the flow instability on the concave surface, a similar analysis for the concave surface was not possible.

Figure 8 shows a profile for $x = 25.4$ centimeters (10 in.) computed by the method just discussed and compared to the profile obtained with a constant static pressure. For the constant-static-pressure case the boundary layer appears to reach a maximum velocity at $y \sim 1.27$ centimeters (0.5 in.) and for the variable case it is reached at $y \sim 0.13$ centimeter (0.05 in.). This latter result makes sense because the highest potential flow velocities at a given value of x are expected to occur near the convexly curved wall rather than the flat wall. From this point outward, the velocity is that of the inviscid flow and should decrease slowly. However, at $y > 0.89$ centimeter (0.35 in.) the velocity begins to drop rapidly, indicating that the approximation for the static-pressure variation is rapidly deteriorating, probably because the streamline pattern is no longer concentric with the curved wall. Hence, the calculated static-pressure rise is too great. Based on figure 8 it can be argued that the edge of the boundary layer is probably at $y = 0.13$ centimeter (0.05 in.) rather than 1.27 centimeters (0.5 in.) and that the flat center part of the profiles in figure 7 for $x = 22.9$, 25.4, 27.9, and 30.5 centimeters (9, 10, 11, and 12 in.) marks the beginning of the essentially inviscid outer flow. Also, in what now appears to be boundary-layer flow ($0 < y < 0.05$), there is a maximum velocity error of less than +1 percent caused by not considering the static-pressure variation.

The conclusion to be drawn from the previous discussion of the curved-wall profiles obtained in the accelerating region is that a knowledge of the static-pressure variation is essential in order to define the flow outside of the rather thin layer where the predominant shear takes place. Within this shear layer the assumption of a constant static pressure appears to be satisfactory. Experimental determination of the boundary-layer profiles in the region of concave wall curvature (in the absence of static-pressure surveys), however, is much more difficult since frictional effects now extend throughout the entire velocity profile and strong secondary flows are known to exist at the wall.

To facilitate comparison of the present results with other data and for the purpose of further analysis, the experimental velocity profiles shown in figure 6 are also presented in table I.

Analysis of Experimental Profiles

It was shown that there was a problem in defining the location of and conditions at the edge of the curved wall accelerating boundary layer. It is not inconceivable that similar difficulties also exist in interpreting the accelerated flat wall profiles. When the pressure gradient is zero, adverse, or only slightly favorable, the semilogarithmic plots of figures 6 and 7 show the existence of a rather well defined outer edge for the profiles. For strong favorable gradients, for example, $x > 20.3$ centimeters (8 in.) on the flat wall, however, the velocity profiles approach the free-stream velocity so slowly that assigning a thickness in terms of 99 percent of the free-stream velocity becomes very arbitrary. Also, in the previous section it was argued that for certain of the curved-wall profiles the boundary-layer edge probably occurred at about the inner 1/10 of the entire velocity profile thickness. Hence, it became necessary to establish some sort of rational criterion for defining the edge of the boundary layer.

To help settle this question, it was decided to examine the distribution of frictional effects in the velocity profiles by comparing an actual measured profile at a given x location with a hypothetical profile that would exist at the same x location in the absence of frictional effects. Thus, regions where frictional effects occurred would be indicated by velocity differences between the two profiles, and regions of negligible friction effects by coincidence of the two profiles. Such a procedure was used in the work described in reference 2, where a given total-pressure profile measured at a given x location was expanded isentropically along streamlines to a static pressure corresponding to some downstream location. In other words, the total pressure was considered constant along a given streamline in calculating the expanded velocity profile. The expanded velocity profile was then compared to the actual measured profile obtained at the downstream location, and the regions of frictional and inviscid flow could be readily identified with regions of velocity difference or identity. For brevity, the term "expanded" is used to mean "expanded isentropically along streamlines."

The comparison of these actual and expanded profiles for the flat wall is presented in figure 9, which shows expanded profiles calculated with the stagnation pressures measured 5.1 centimeters (2 in.) upstream of each actual profile. At $x = 5.1$ and 10.2 centimeters (2 and 4 in.) the flow acceleration is relatively small, and a comparison of the actual and expanded profiles in this region shows that very small velocity differences extend throughout most of the profile and indicate frictional development from the wall to the free stream. Beginning at $x = 15.2$ centimeters (6 in.) an appreciable velocity difference appears near the wall, and this increases rapidly as the flow acceleration rises. At $x > 20.3$ centimeters (8 in.) all the velocity differences are confined to a narrow region adjacent to the wall, $y \leq 0.25$ centimeter (0.10 in.), the outer 80 percent of the velocity profiles indicating negligible differences, hence negligible shear gradients and

negligible shear. From this it is concluded that for the rapidly accelerating part of the flow the outer portions of the velocity profiles reflect the earlier history of the boundary layer and are accurately predictable from inviscid flow relations. Presumably the turbulence in the outer portions of these velocity profiles has become uncorrelated, that is, the Reynolds stresses have gone to zero. As a result of the total-pressure gradient normal to the flow direction, the flow is considered rotational in the outer region.

At this point it may be advisable to comment on the accuracy of the boundary-layer measurements. Because a dimensionless velocity is used in figure 9, all the profiles must terminate at $u/u_\infty = 1$, and hence some question may arise concerning the coincidence of the outer part of the expanded and actual velocity profiles. A comparison of the absolute velocities, however, indicated differences of at most ±0.6 or 0.9 meter per second (±2 or 3 ft/sec) (less than 1/2 percent), which is the experimental accuracy of the measurements. Accuracy of the profiles in the inner regions is nominally equal to that in the outer.

Although the step size selected to compare the actual and expanded profiles was 5 centimeters (2 in.), the same general conclusions followed when the step size was reduced to 2.54 centimeters (1 in.) or increased to 10.16 centimeters (4 in.). For step sizes of 15.24 centimeters (6 in.) or more it was not possible to bracket a region of boundary layer all of which was highly accelerated. As was expected in these instances, the outer portions of the velocity profile experienced frictional development and could not be represented by an isentropic expansion along streamlines.

Another observation to be made about the actual velocity profiles of figure 9 concerns the apparent disappearance of the wake region (0.25 cm $< y <$ 1.3 cm or 0.10 in. $< y <$ 0.50 in.) as the acceleration increases. Whereas the disappearance of the wake region in the outer part of the profile is to be expected, a development in the inner part of the profile suggests the establishment of a new wake region much closer to the wall (0.038 cm $< y <$ 0.13 cm or 0.015 in. $< y <$ 0.05 in). This conclusion is based on the slight upward concavity of the actual velocity profiles at $x \geq 20.3$ centimeters (8 in.) for values of $y < 0.13$ centimeter (0.05 in.). The implication is that, when the shear gradient becomes sufficiently weak in the outer part of the velocity profile because of acceleration, a new wake region will form nearer to the wall, which will supply turbulent energy for a much thinner turbulent boundary layer by entraining air from the inviscid rotational layer. The existence of such a new wake region much closer to the wall has also been suggested by turbulent intermittency measurements in a strongly accelerated turbulent boundary layer (refs. 3 and 5). These latter results showed a conventional turbulent intermittency distribution in a small region near the wall nested inside of a much larger intermittency distribution corresponding to the entire velocity profile. The picture of the turbulent boundary layer in accelerated flow evolving here requires first a reduction in boundary-layer mass flow, that is, negative entrainment or thinning of the frictional boundary layer, in the region of large acceleration. This is followed by positive

entrainment first from the inviscid rotational layer and later from the free stream as the acceleration diminishes. A familiar analogy in supersonic flow is the boundary-layer development through a shock layer over a blunted body.

Figure 10 shows a comparison of actual and expanded profiles measured on the curved wall at three positions in the accelerating part of the flow. The expanded profiles were calculated from total-pressure profiles measured 2.54 centimeters (1 in.) upstream of each respective actual profile (rather than 5.1 cm or 2 in. upstream, as in fig. 9) because of the very rapid changes due to the larger flow accelerations. Static pressures were assumed constant perpendicular to the wall to simplify and expedite comparisons. It is hoped that use of a constant static, albeit incorrect, pressure distribution for both the actual and expanded profiles will not invalidate this comparison. Again, the outer part of the profiles ($y \geq 0.13$ cm or 0.05 in.) is accurately described by inviscid flow along streamlines, and the frictional effects are confined to a much thinner layer near the wall having larger velocity gradients than those observed on the flat wall. At $x = 25.4$ centimeters (10 in.) the frictional effects appear confined to a layer about 0.089 centimeter (0.035 in.) thick compared to a total velocity profile of at least 1.3 centimeters (0.5 in.) or only 7 percent of the entire velocity profile.

Although a comparison of the actual and expanded profiles in the concave curvature region (adverse pressure gradient) was attempted, a quantitative comparison is out of the question since it was not possible to define the streamlines in the secondary flow region near the wall.

Theoretical Prediction of Profiles and Comparison With Experiment

Theoretical turbulent velocity profiles were computed for the flat wall by using the differential technique of reference 6 and are presented in figure 11, where they are compared with the experimental profiles of figure 6. The theoretical computation was initialized by using the measured boundary-layer profile at $x = 0$ and assuming a negligible free-stream turbulence level.

A comparison of the experimental theoretical profiles shows that the latter duplicate the general trends of the measured profiles remarkably well, although no account was taken of an inviscid rotational region outside the frictional boundary layer in the theory. Both sets of profiles indicate a disappearance of the outer wake region and an increase in velocity near the wall at increasing distances downstream, that is, with increasing acceleration. There is a difference between experiment and theory, however, which may be significant in this accelerated region. It concerns the upward concavity of the experimental profiles at $x \geq 15.2$ centimeters (6 in.) in the neighborhood of the wall (0.008 cm $< y < 0.08$ cm or 0.003 in. $< y < 0.03$ in.) resulting in the establishment of a new wake region near the wall which was alluded to previously. The theoretical profiles,

on the other hand, show a slight downward concavity or at most a linear variation in this region for all the profiles. If the experimental profiles are correct and typical of accelerated flows, the theoretical model of the turbulent boundary layer may need some modification which will establish the edge of the frictional boundary layer much closer to the wall. In view of the rather good agreement between experimental and theoretical velocity profiles indicated in figure 11, such a modification may not be worth the effort in this instance. This does not preclude the existence of situations where a more accurate modeling is required.

Another differentiation between the experimental and theoretical profiles becomes apparent if the theoretical profiles are expanded isentropically in the same manner as the measured profiles were in the previous section. These are shown in figure 12 for $x = 20.3$, 25.4, 30.5, and 35.6 centimeters (8, 10, 12, and 14 in.), the profiles for $x < 20.3$ centimeters (8 in.) being omitted because they were almost identical to the experimental profiles presented in figure 9(a). A comparison of these profiles with the experimental profiles of figure 9(b) shows that the trends exhibited by both sets of profiles are remarkably similar. A closer examination of these figures, however, shows that the actual and expanded profiles approach each other somewhat more abruptly (for $y \geq 0.23$ cm or 0.09 in.) when the experimental profiles are compared in figure 9(b) than when the theoretical profiles are compared in figure 12. In fact, some small velocity differences persist nearly to the free stream for the case of the theoretical profiles; these differences indicate the presence of a small amount of shear.

In view of the differences between the measured and computed velocity profiles just discussed, it is felt that some new criterion is required in the theory to define the edge of the boundary layer, where frictional effects are present, and to distinguish this point from the free stream, which may be considerably farther removed from the wall. It may also turn out that, when a proper choice of the boundary-layer outer edge is made, the upper concave curvature of the measured profiles discussed previously will be predicted by the theoretical profiles also.

Because of uncertainties in analyzing the experimental and theoretical profiles on the curved wall, detailed quantitative comparisons cannot be made. These uncertainties include static-pressure variations normal to the surface and the destabilizing effect of the initial turning, which results in the establishment of secondary flows on the curved wall. Qualitatively, it can be said that the application of the theory of reference 6 reproduces the trends of the experimental curved-wall profiles of figure 7, but in general underestimates the velocities near the wall. This happens because in the real flow the low-energy air at the wall is displaced laterally by the faster moving air of the free stream in the region of compressive (concave) turning.

Comparison of Experimental and Theoretical Boundary-Layer Thickness

A comparison of the present experimental results, in terms of displacement, momentum, and velocity thicknesses δ^*, θ, and δ, respectively, with the predictions of the integral technique of reference 7 and the differential technique of reference 6 is given in this section.

Figure 13 shows a comparison of the experimental boundary-layer development on the flat and curved walls with the predictions of reference 7. Displacement and momentum thicknesses have the conventional two-dimensional compressible formulations with the upper integration limit taken to be the free stream. The velocity thickness is taken at the point where $u/u_\infty = 0.99$. The velocity profiles assumed in applying reference 7 were power profiles having 1/8 and 1/7 powers corresponding to the initial profiles measured on the flat and curved walls, respectively.

Figure 13(a), for the flat wall, shows very good agreement between experiment and theory throughout except for the velocity thickness, which diverges rapidly beginning at x = 15.2 centimeters (6 in.). The agreement between experiment and predictions on the curved wall, figure 13(b), while not as good as for the flat wall, reflects the same general trends. Again, the velocity thickness distribution shows the largest variations. This variation results from assuming a constant power profile along the channel length in reference 7, whereas the actual power varies from about 1/7 to 1/30. Other discrepancies for the curved wall are attributable to the secondary flows and static-pressure variations which are known to exist.

The comparison between the measured thicknesses and those predicted by the differential technique of reference 6 is shown in figure 14. Only the boundary-layer development along the flat wall was computed for this comparison. Very good agreement is again obtained for both the momentum and displacement thicknesses. In addition, the predicted velocity thickness now agrees well with the measured values, both being based on the thickness at the 99 percent velocity distance with the free stream assumed to be the outer boundary condition.

CONCLUDING REMARKS

The picture of the accelerating flow turbulent boundary layer which evolves from this study has some characteristics which distinguish if from more conventional turbulent-boundary-layer models. These are

1. The velocity profile has two distinct regions: an inner frictional layer composed of the usual "law of the wall" and "wake" regions, and an outer inviscid rotational layer resulting from the early turbulent-boundary-layer history.

2. As a result of the two-layer model for the accelerated turbulent velocity profile, the outer boundary condition for the inner frictional layer is determined by the inviscid rotational layer rather than by the free stream.

3. During some period of its rapid acceleration the turbulent boundary layer experiences a negative entrainment (expulsion of mass flow from the boundary layer) which is followed by a positive entrainment, first of the inviscid rotational layer and later of the free stream as the acceleration diminishes.

4. There is a suggestion of a wakelike region for the frictional boundary layer even when it has become severely thinned by acceleration. The function of this wake region is to entrain high-energy air from the outer rotational layer in the same manner as the wake region of a conventional turbulent boundary layer entrains the free stream.

It should be pointed out that the characteristics just enumerated are for a particular accelerating turbulent boundary layer, that is, one having sufficient thickness as well as sufficient acceleration, as was mentioned previously.

Lewis Research Center,
National Aeronautics and Space Administration,
Cleveland, Ohio, September 9, 1971,
132-15.

REFERENCES

1. Boldman, Donald R.; Schmidt, James F.; and Fortini, Anthony: Turbulence, Heat-Transfer, and Boundary Layer Measurements in a Conical Nozzle with a Controlled Inlet Velocity Profile. NASA TN D-3221, 1966.

2. Brinich, Paul F.; and Neumann, Harvey E.: Some effects of Acceleration on the Turbulent Boundary Layer. AIAA J., vol. 8, no. 5, May 1970, pp. 987-989.

3. Boldman, Donald R.; Neumann, Harvey E.; and Ehlers, Robert C.: Velocity, Intermittency, and Turbulence Intensity Measurements in the Boundary Layer of an Accelerated Flow. NASA TN D-6043, 1970.

4. Schraub, F. A.; and Kline, S. J.: A Study of the Structure of the Turbulent Boundary Layer with and without Longitudinal Pressure Gradients. Rep. MD-12, Stanford Univ. (AFOSR-67-0605, AD-646989, Mar. 1965.

5. Boldman, Donald R.; and Neumann, Harvey E.: Intermittency in a Highly Accelerated Boundary Layer. AIAA J., vol. 8, no. 10, Oct. 1970, pp. 1899-1900.

6. Kays, M. W.; Moffat, R. J.; Kearney, D. W.; and Loyd, R. J.: The Effect of Free-Stream Turbulence on Heat Transfer to a Strongly Accelerated Turbulent Boundary Layer. Proceedings of the 1970 Heat Transfer and Fluid Mechanics Institute. Turgut Sarpkaya, ed., Stanford University Press, 1970, pp. 3-14.

7. Ellicott, David G.; Bartz, Donald R.; and Silver, Sidney: Calculation of Turbulent Boundary-Layer Growth and Heat Transfer in Axi-Symmetric Nozzles. Tech. Rep. 32-387, Jet Propulsion Lab, Calif. Inst. Tech., Feb. 15, 1963.

TABLE I. - EXPERIMENTAL VELOCITY DISTRIBUTIONS ON FLAT WALL

(a) Axial position, 0 centimeter (0 in.); stagnation pressure, 95 835 newtons per square meter (28.3 in. Hg); static pressure, 81 443 newtons per square meter (24.0 in. Hg); stagnation temperature, 278.3 K (501.0° R)

Distance normal to wall		Velocity	
cm	in.	m/sec	ft/sec
0.0076	0.0030	86.33	283.23
0.0102	0.0040	89.75	294.46
0.0127	0.0050	93.03	305.22
0.0178	0.0070	97.55	320.05
0.0254	0.0100	102.16	335.18
0.0330	0.0130	105.63	346.54
0.0457	0.0180	109.85	360.39
0.0584	0.0230	113.04	370.85
0.0838	0.0330	117.76	386.35
0.1092	0.0430	121.75	399.43
0.1600	0.0630	127.32	417.70
0.2108	0.0830	131.66	431.94
0.2616	0.1030	135.60	444.87
0.3124	0.1230	138.29	453.71
0.3886	0.1530	142.21	466.56
0.5156	0.2030	148.04	485.68
0.6426	0.2530	152.41	500.02
0.7696	0.3030	157.17	515.66
0.8966	0.3530	159.94	524.74
1.0236	0.4030	161.75	530.68
1.2776	0.5030	164.06	538.25
1.5316	0.6030	164.59	539.98
1.7856	0.7030	164.59	539.98
2.2936	0.9030	164.59	539.98
3.0556	1.2030	164.59	539.98
4.0716	1.6030	164.59	539.98
5.0876	2.0030	164.59	539.98

(b) Axial position, 5.08 centimeters (2.0 in.); stagnation pressure, 96 140 newtons per square meter (28.4 in. Hg); static pressure, 81 273 newtons per square meter (24.0 in. Hg); stagnation temperature, 294.4 K (530.0° R)

Distance normal to wall		Velocity	
cm	in.	m/sec	ft/sec
0.0076	0.0030	89.84	294.75
0.0102	0.0040	93.13	305.53
0.0127	0.0050	95.94	314.76
0.0152	0.0060	98.32	322.58
0.0178	0.0070	99.99	328.05
0.0203	0.0080	101.62	333.40
0.0254	0.0100	104.49	342.80
0.0330	0.0130	107.57	352.91
0.0457	0.0180	112.00	367.46
0.0584	0.0230	115.12	377.70
0.0711	0.0280	117.60	385.84
0.0838	0.0330	119.76	392.91
0.1092	0.0430	123.42	404.91
0.1346	0.0530	126.20	414.04
0.1600	0.0630	128.91	422.93
0.2108	0.0830	133.19	436.99
0.2616	0.1030	136.63	448.27
0.3124	0.1230	139.97	459.21
0.4140	0.1630	145.51	477.39
0.5156	0.2030	149.99	492.09
0.6172	0.2430	153.91	504.95
0.7188	0.2830	157.51	516.77
0.8204	0.3230	160.46	526.43
0.9220	0.3630	162.80	534.11
1.0236	0.4030	164.89	539.33
1.2776	0.5030	166.31	545.62
1.5316	0.6030	167.17	548.45
1.7856	0.7030	167.17	548.45
2.5476	1.0030	167.17	548.45
3.8176	1.5030	167.17	548.45
5.0876	2.0030	167.17	548.45

TABLE I. - Continued. EXPERIMENTAL VELOCITY DISTRIBUTIONS ON FLAT WALL

(c) Axial position, 10.16 centimeters (4.0 in.); stagnation pressure, 93 769 newtons per square meter (27.7 in. Hg); static pressure, 78 530 newtons per square meter (23.2 in. Hg); stagnation temperature, 294.4 K (530° R)

Distance normal to wall		Velocity	
cm	in.	m/sec	ft/sec
0.0076	0.003C	97.89	321.16
0.0102	0.004C	100.98	331.30
0.0127	0.005C	103.64	340.03
0.0152	0.006C	105.90	347.45
0.0203	0.008C	109.04	357.74
0.0279	0.011C	112.96	370.62
0.0381	0.015C	115.88	380.17
0.0483	0.019C	118.70	389.44
0.0584	0.023C	121.18	397.56
0.0838	0.033C	125.43	411.52
0.1092	0.043C	129.26	424.09
0.1600	0.063C	134.63	441.71
0.2108	0.083C	138.83	455.49
0.2616	0.103C	141.77	465.12
0.3378	0.133C	145.92	478.73
0.4140	0.163C	149.71	491.17
0.5156	0.203C	153.77	504.50
0.6426	0.253C	158.66	520.52
0.7696	0.303C	163.34	535.88
0.8966	0.353C	166.06	544.81
1.0236	0.403C	168.36	552.38
1.2776	0.503C	170.97	560.92
1.5316	0.603C	171.66	563.17
2.0396	0.803C	171.83	563.73
2.5476	1.003C	171.83	563.73
3.5636	1.403C	171.83	563.73
4.5796	1.803C	171.83	563.73
5.0876	2.003C	171.83	563.73

(d) Axial position, 15.24 centimeters (6.0 in.); stagnation pressure, 94 480 newtons per square meter (27.9 in. Hg); static pressure, 77 311 newtons per square meter (22.8 in. Hg); stagnation temperature, 287.2 K (517.0° R)

Distance normal to wall		Velocity	
cm	in.		ft/sec
0.0076	0.0030	110.48	362.46
0.0102	0.0040	113.21	371.43
0.0127	0.0050	115.58	379.20
0.0152	0.0060	117.32	384.90
0.0203	0.0080	120.70	396.00
0.0330	0.0130	126.10	413.70
0.0457	0.0180	130.47	428.04
0.0584	0.0230	134.17	440.20
0.0838	0.0330	138.92	455.78
0.1092	0.0430	142.57	467.76
0.1600	0.0630	148.47	487.11
0.2108	0.0830	152.23	499.46
0.2616	0.1030	155.08	508.78
0.3378	0.1330	159.01	521.70
0.4140	0.1630	162.26	532.34
0.5156	0.2030	166.14	545.09
0.6426	0.2530	170.60	559.73
0.7696	0.3030	173.54	569.37
0.8966	0.3530	176.58	579.32
1.0236	0.4030	179.05	587.42
1.2776	0.5030	181.47	595.36
1.5316	0.6030	182.26	597.97
2.0396	0.8030	182.42	598.49
2.5476	1.0030	182.42	598.49
3.0556	1.2030	182.42	598.49
3.5636	1.4030	182.42	598.49
4.0716	1.6030	182.42	598.49
4.5796	1.8030	182.42	598.49

TABLE I. - Continued. EXPERIMENTAL VELOCITY DISTRIBUTIONS ON FLAT WALL

(e) Axial position, 20.32 centimeters (8.0 in.); stagnation pressure, 93 871 newtons per square meter (27.7 in. Hg); static pressure, 73 315 newtons per square meter (21.7 in. Hg); stagnation temperature, 296.7 K (534.0° R)

Distance normal to wall		Velocity	
cm	in.	m/sec	ft/sec
0.0076	0.003C	124.89	409.75
0.0102	0.004C	128.74	422.38
0.0127	0.005C	131.93	432.84
0.0178	0.007C	136.79	448.78
0.0254	0.010C	142.15	466.36
0.0330	0.013C	146.57	480.87
0.0457	0.018C	151.48	496.97
0.0584	0.023C	155.76	511.02
0.0838	0.033C	161.49	529.84
0.1092	0.043C	165.61	543.35
0.1600	0.063C	170.89	560.65
0.2108	0.083C	174.87	573.72
0.2616	0.103C	177.34	581.81
0.3632	0.143C	182.29	598.05
0.4648	0.183C	186.23	611.00
0.6172	0.243C	190.99	626.61
0.7696	0.303C	194.52	638.17
1.0236	0.403C	198.67	651.81
1.2776	0.503C	199.83	655.62
1.5316	0.603C	200.12	656.57
2.0396	0.803C	200.41	657.51
2.5476	1.003C	200.41	657.51
3.0556	1.203C	200.41	657.51
3.5636	1.403C	200.41	657.51
4.0716	1.603C	200.41	657.51
4.5796	1.803C	200.41	657.51
5.1638	2.033C	200.41	657.51

(f) Axial position, 25.40 centimeters (10.0 in.); stagnation pressure, 94 074 newtons per square meter (27.8 in. Hg); static pressure, 66 712 newtons per square meter (19.7 in. Hg); stagnation temperature, 305.6 K (550.0° R)

Distance normal to wall		Velocity	
cm	in.	m/sec	ft/sec
0.0076	0.0030	160.38	526.19
0.0102	0.0040	163.66	536.94
0.0127	0.0050	166.85	547.40
0.0178	0.0070	172.17	564.87
0.0229	0.0090	176.30	578.42
0.0279	0.0110	179.92	590.28
0.0330	0.0130	183.24	601.20
0.0457	0.0180	189.63	622.16
0.0584	0.0230	195.21	640.44
0.0838	0.0330	201.63	661.53
0.1092	0.0430	205.79	675.15
0.1600	0.0630	211.40	693.58
0.2108	0.0830	215.24	706.18
0.2616	0.1030	218.01	715.26
0.3632	0.1430	221.92	728.08
0.4648	0.1830	224.93	737.96
0.5664	0.2230	227.37	745.95
0.6680	0.2630	229.63	753.37
0.7696	0.3030	231.60	759.85
1.0236	0.4030	234.63	769.78
1.2776	0.5030	235.94	774.07
1.5316	0.6030	236.29	775.23
2.0396	0.8030	236.29	775.23
2.5476	1.0030	236.29	775.23
3.0556	1.2030	236.29	775.23
3.5636	1.4030	236.29	775.23
4.0716	1.6030	236.29	775.23

TABLE I. - Concluded. EXPERIMENTAL VELOCITY DISTRIBUTION ON FLAT WALL

(g) Axial position, 30.48 centimeters (12.0 in.); stagnation pressure, 92 584 newtons per square meter (27.3 in. Hg); static pressure, 55 367 newtons per square meter (16.4 in. Hg); stagnation temperature, 301.7 K (543.0° R)

Distance normal to wall		Velocity	
cm	in.	m/sec	ft/sec
0.0076	0.003C	197.74	648.76
0.0102	0.004C	201.39	660.72
0.0127	0.005C	206.20	676.52
0.0178	0.007C	214.12	702.48
0.0229	0.009C	219.77	721.03
0.0279	0.011C	224.55	736.73
0.0330	0.013C	229.31	752.32
0.0457	0.018C	237.88	780.44
0.0584	0.023C	244.30	801.50
0.0711	0.028C	249.51	818.60
0.0838	0.033C	253.28	830.96
0.1092	0.043C	258.72	848.81
0.1600	0.063C	265.39	870.70
0.2108	0.083C	269.03	882.63
0.2616	0.103C	271.71	891.43
0.3632	0.143C	275.37	903.44
0.4648	0.183C	277.41	910.13
0.5664	0.223C	279.42	916.72
0.6680	0.263C	280.90	921.59
0.7696	0.303C	282.37	926.39
1.0236	0.403C	284.39	933.02
1.2776	0.503C	284.96	934.90
1.5316	0.603C	285.24	935.83
2.0396	0.803C	285.34	936.14
2.5476	1.003C	285.43	936.45
3.0556	1.203C	285.43	936.45
3.5636	1.403C	285.43	936.45
4.0716	1.603C	285.43	936.45

(h) Axial position, 35.56 centimeters (14.0 in.); stagnation pressure, 93 227 newtons per square meter (27.5 in. Hg); static pressure, 43 786 newtons per square meter (12.9 in. Hg); stagnation temperature, 301.7 K (543.0° R)

Distance normal to wall		Velocity	
cm	in.	m/sec	ft/sec
0.0076	0.0030	230.84	757.35
0.0102	0.0040	239.72	786.47
0.0127	0.0050	246.02	807.14
0.0178	0.0070	255.44	838.04
0.0229	0.0090	263.31	863.89
0.0279	0.0110	269.62	884.59
0.0330	0.0130	274.84	901.69
0.0457	0.0180	285.70	937.34
0.0584	0.0230	293.88	964.17
0.0711	0.0280	300.37	985.47
0.0838	0.0330	305.72	1003.01
0.1092	0.0430	313.48	1028.49
0.1346	0.0530	319.25	1047.42
0.1600	0.0630	322.59	1058.38
0.2108	0.0830	327.27	1073.73
0.2616	0.1030	329.75	1081.86
0.3632	0.1430	332.50	1090.89
0.4648	0.1830	334.33	1096.89
0.5664	0.2230	335.82	1101.78
0.6680	0.2630	337.07	1105.86
0.7696	0.3030	337.99	1108.90
1.0236	0.4030	339.44	1113.66
1.2776	0.5030	339.74	1114.62
1.5316	0.6030	339.89	1115.12
2.0396	0.8030	340.04	1115.62
2.5476	1.0030	340.04	1115.62
3.0096	1.3030	340.04	1115.62
4.0716	1.6030	340.04	1115.62

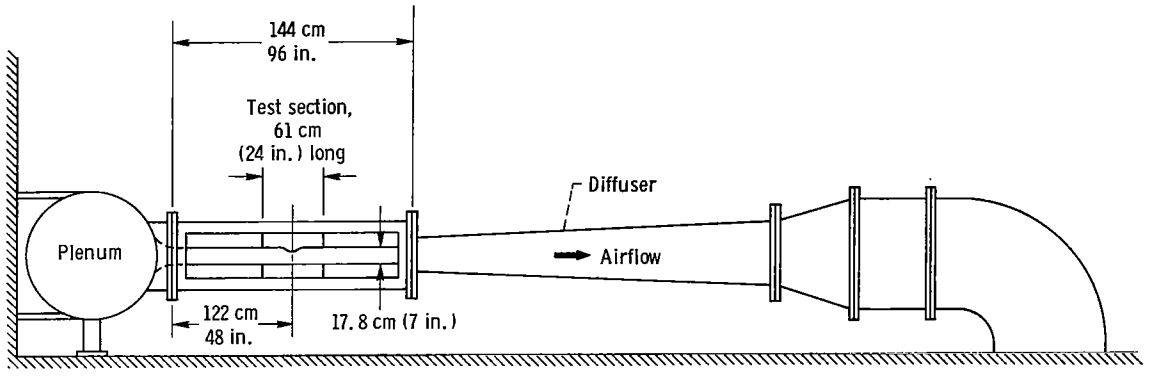

Figure 1. - General arrangement of test facility.

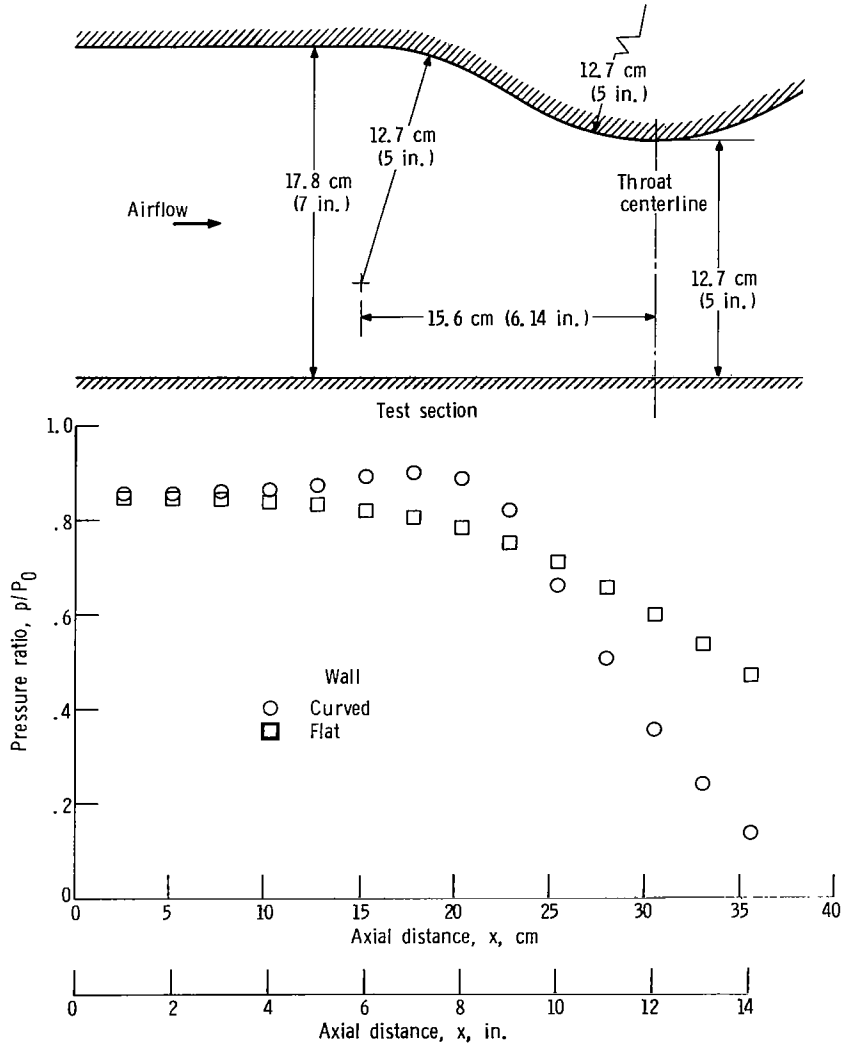

Figure 2. - Test section and static-pressure distribution.

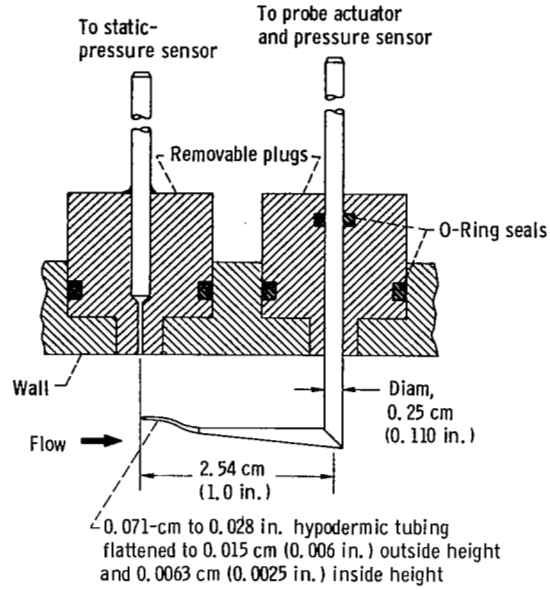

Figure 3. - Probe and installation in wall.

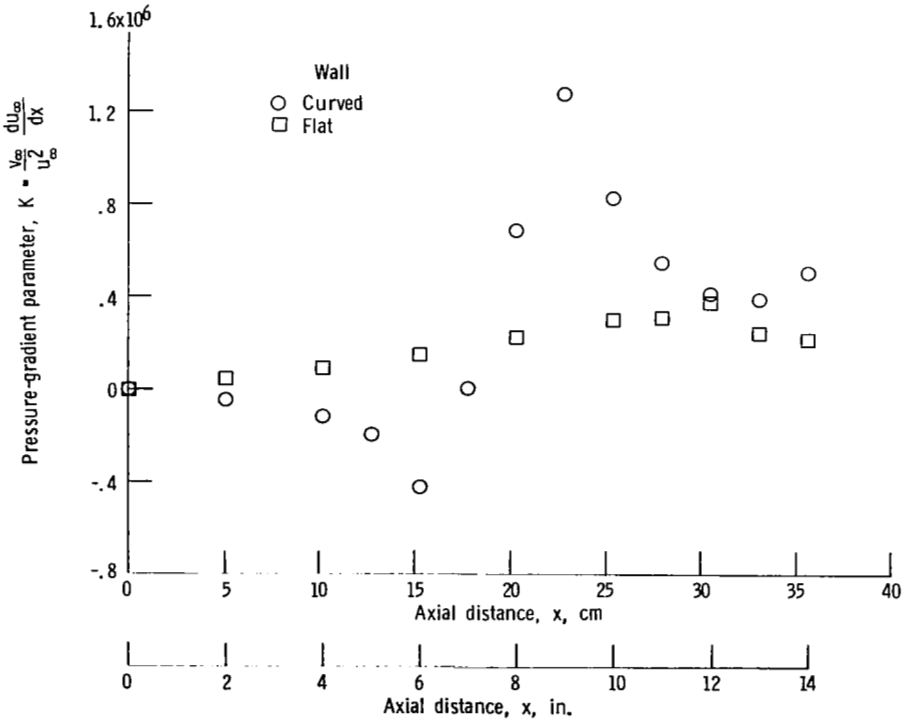

Figure 4. - Variation of pressure-gradient parameter K.

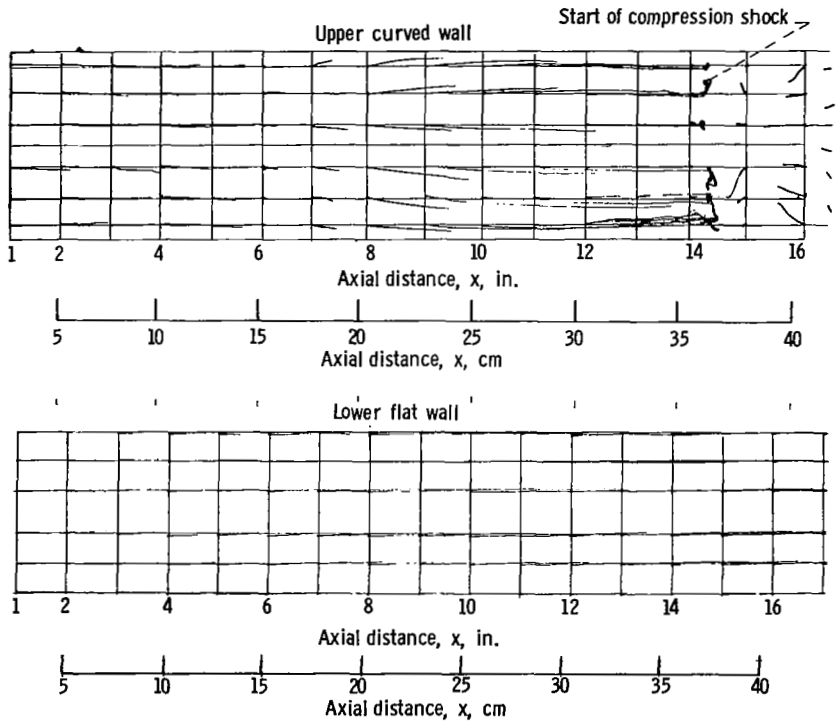

Figure 5. - Flow direction traces on curved and flat wall.

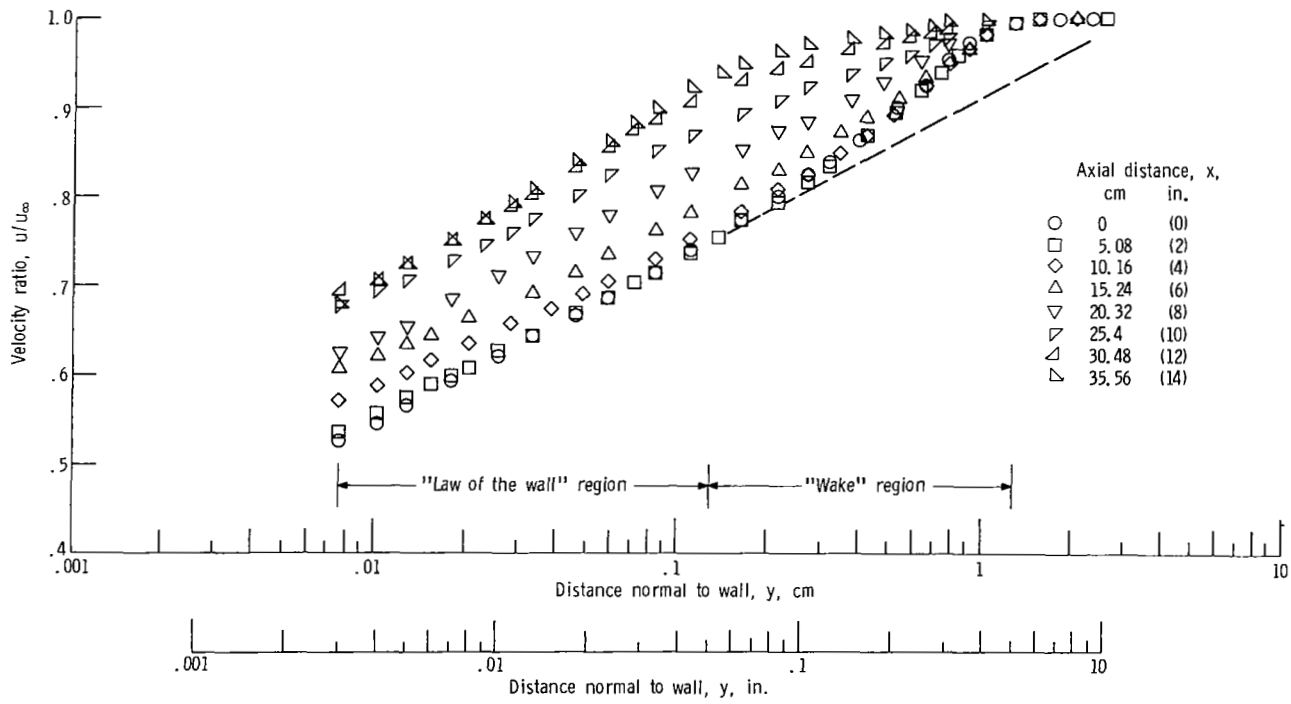

Figure 6. - Experimental velocity profiles along flat wall.

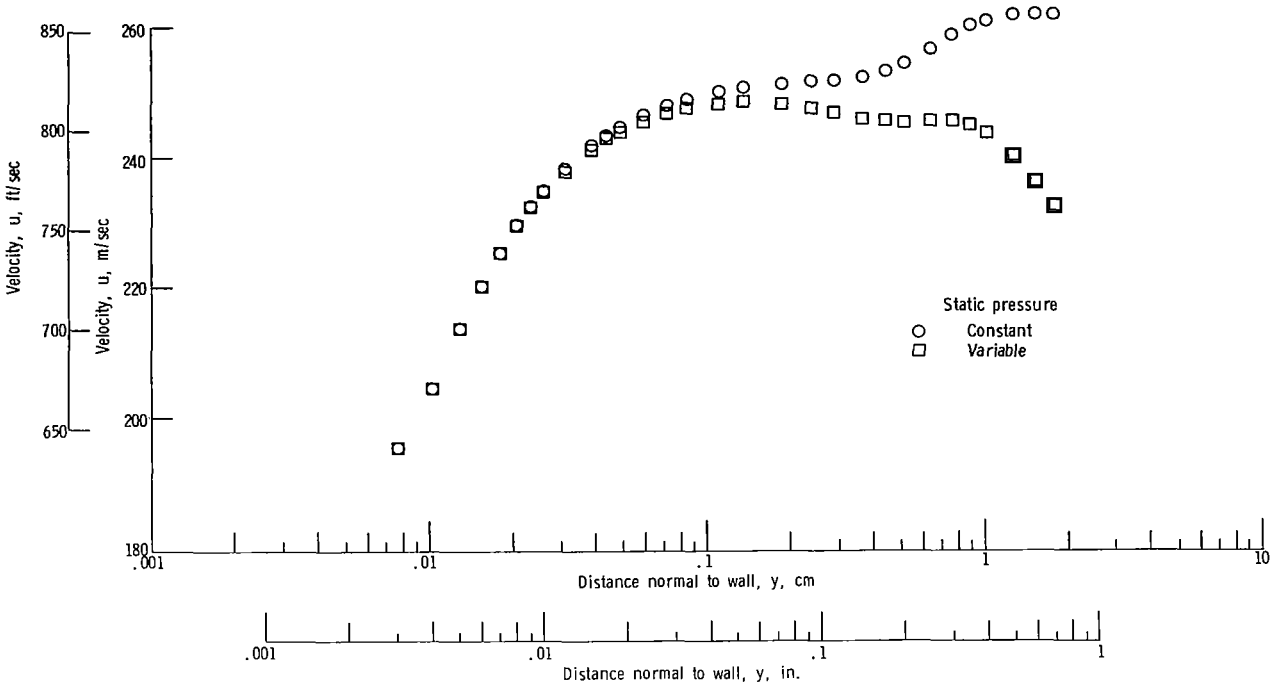

Figure 8. - Effect of variable static pressure on curved wall profile at axial distance of 25.4 centimeters (10 in.).

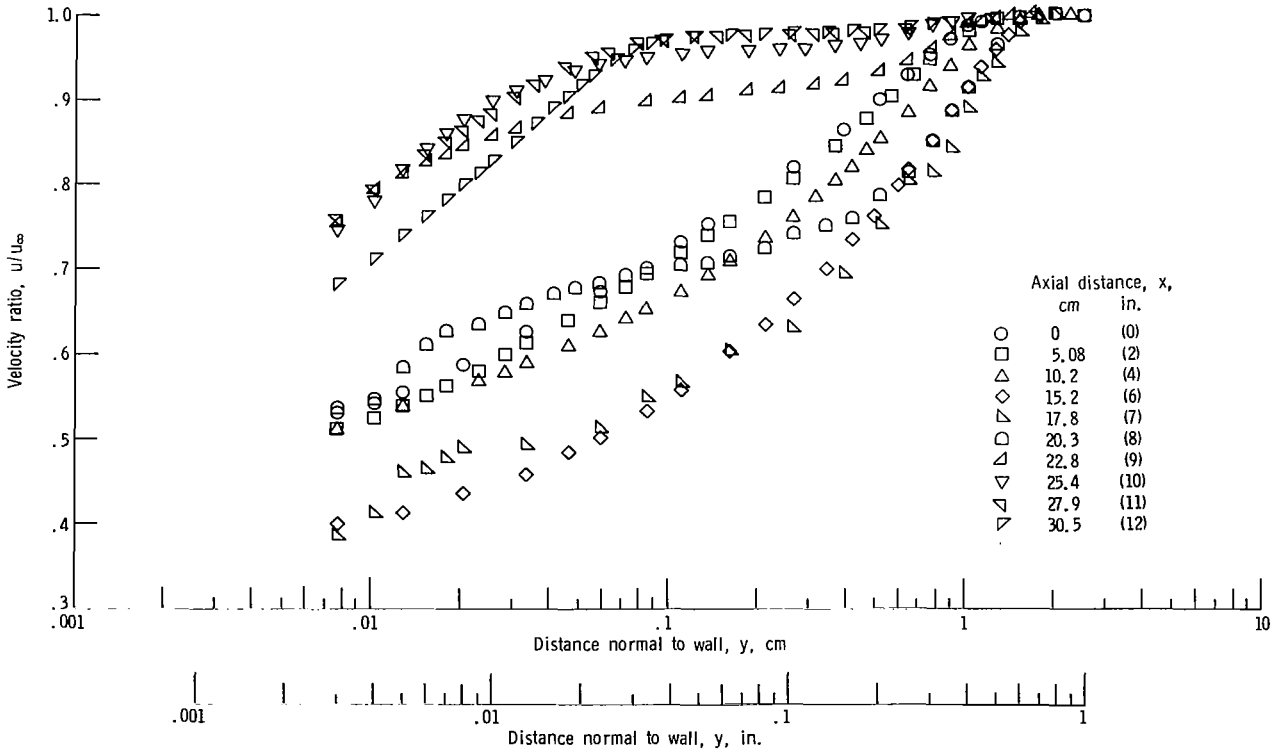

Figure 7. - Velocity profiles along curved wall.

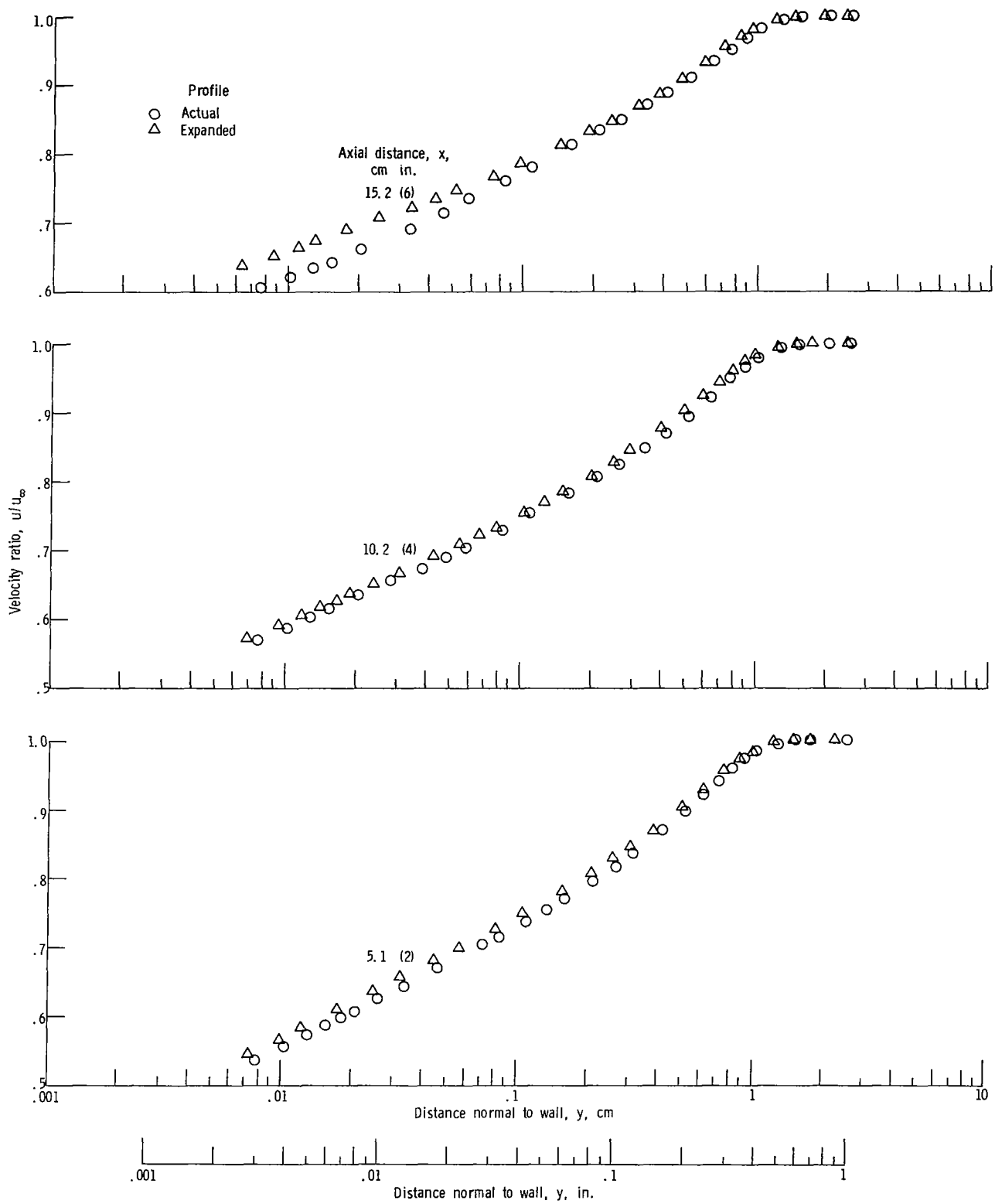

(a) Axial distances of 15.2, 10.2, and 5.1 centimeters (6, 4, and 2 in.).

Figure 9. - Actual and expanded profiles on flat wall.

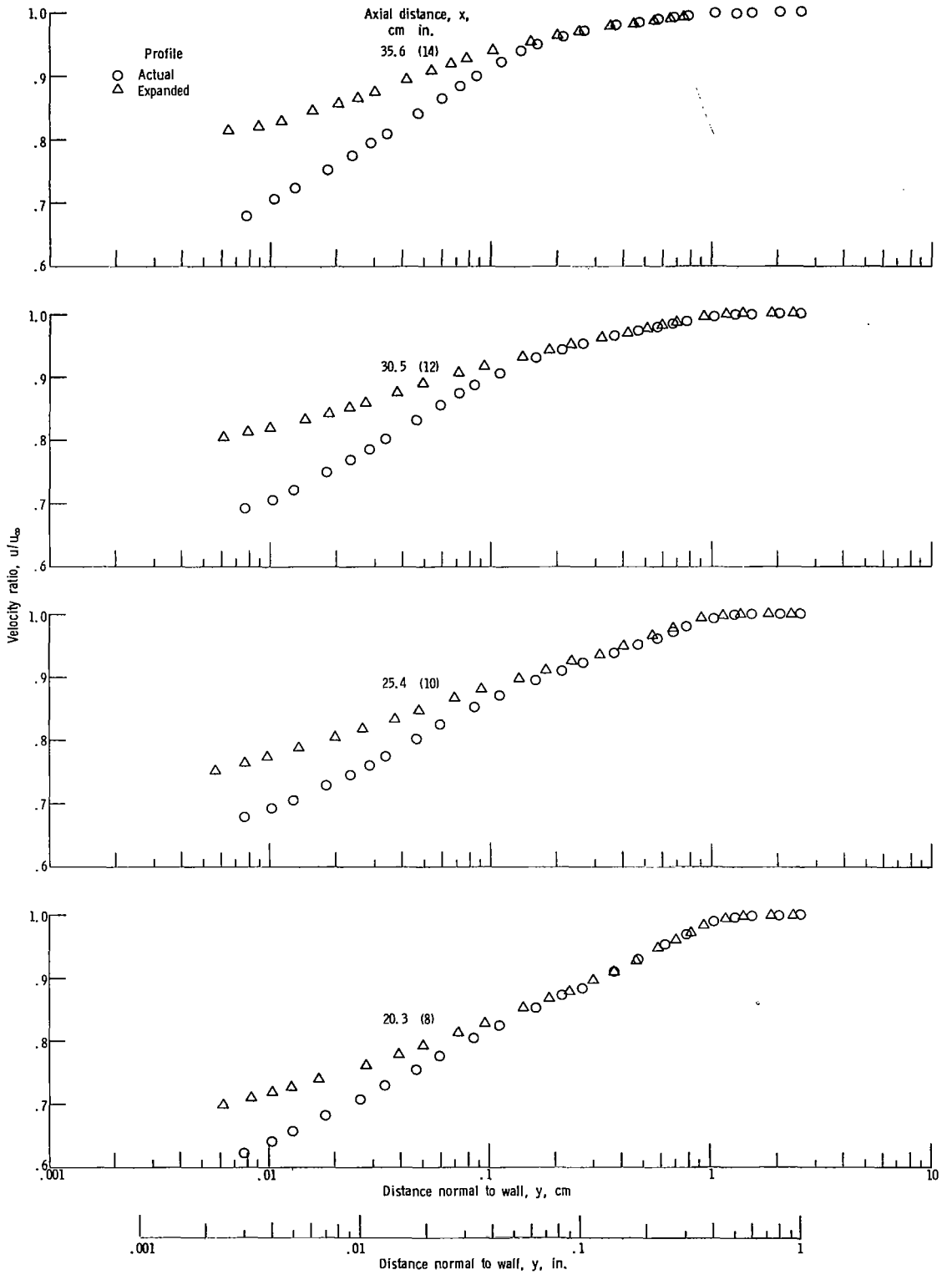

(b) Axial distances of 35.6, 30.5, 25.4, and 20.3 centimeters (14, 12, 10, and 8 in.).

Figure 9. - Concluded.

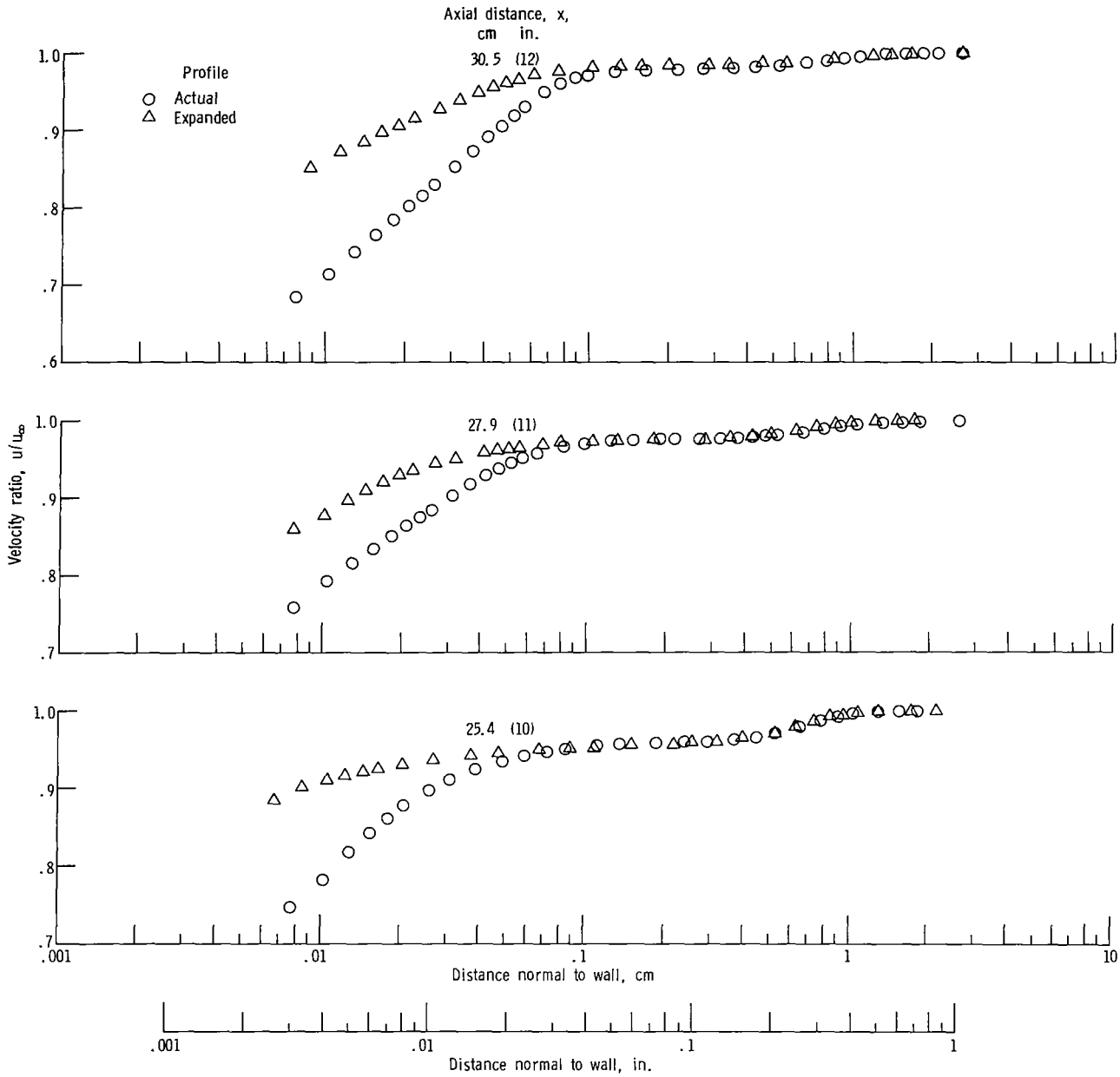

Figure 10. - Actual and expanded profiles on curved wall.

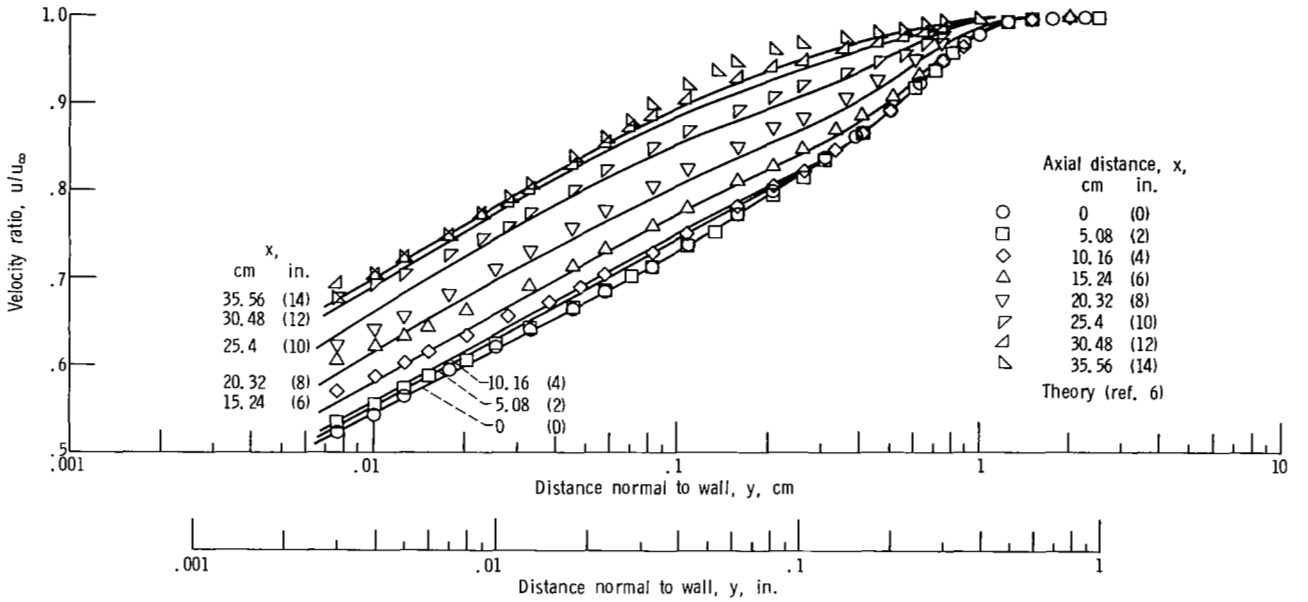

Figure 11. - Comparison of theoretical (ref. 6) and experimental profiles along flat wall.

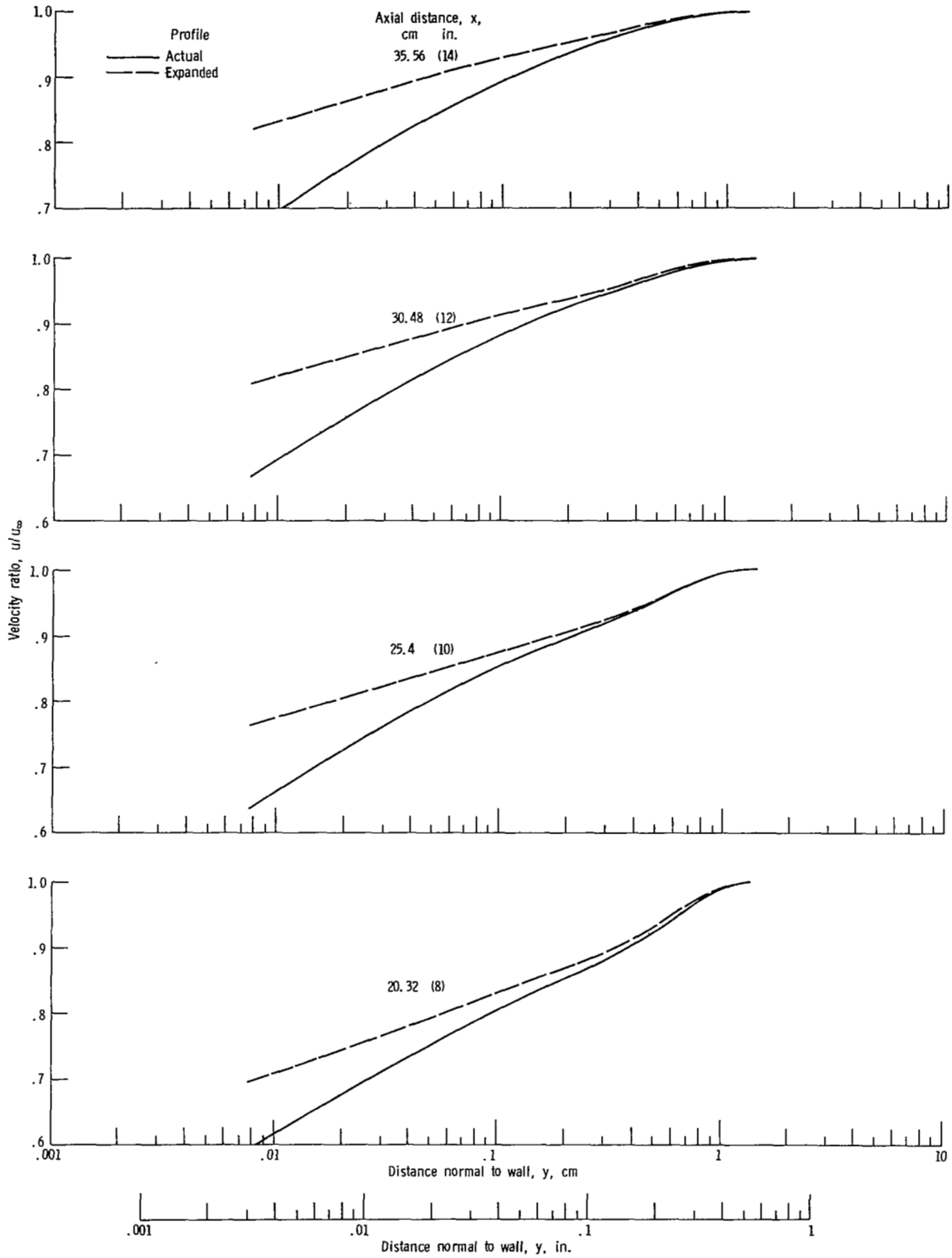

Figure 12. - Theoretical, actual, and expanded profiles on flat wall from reference 6.

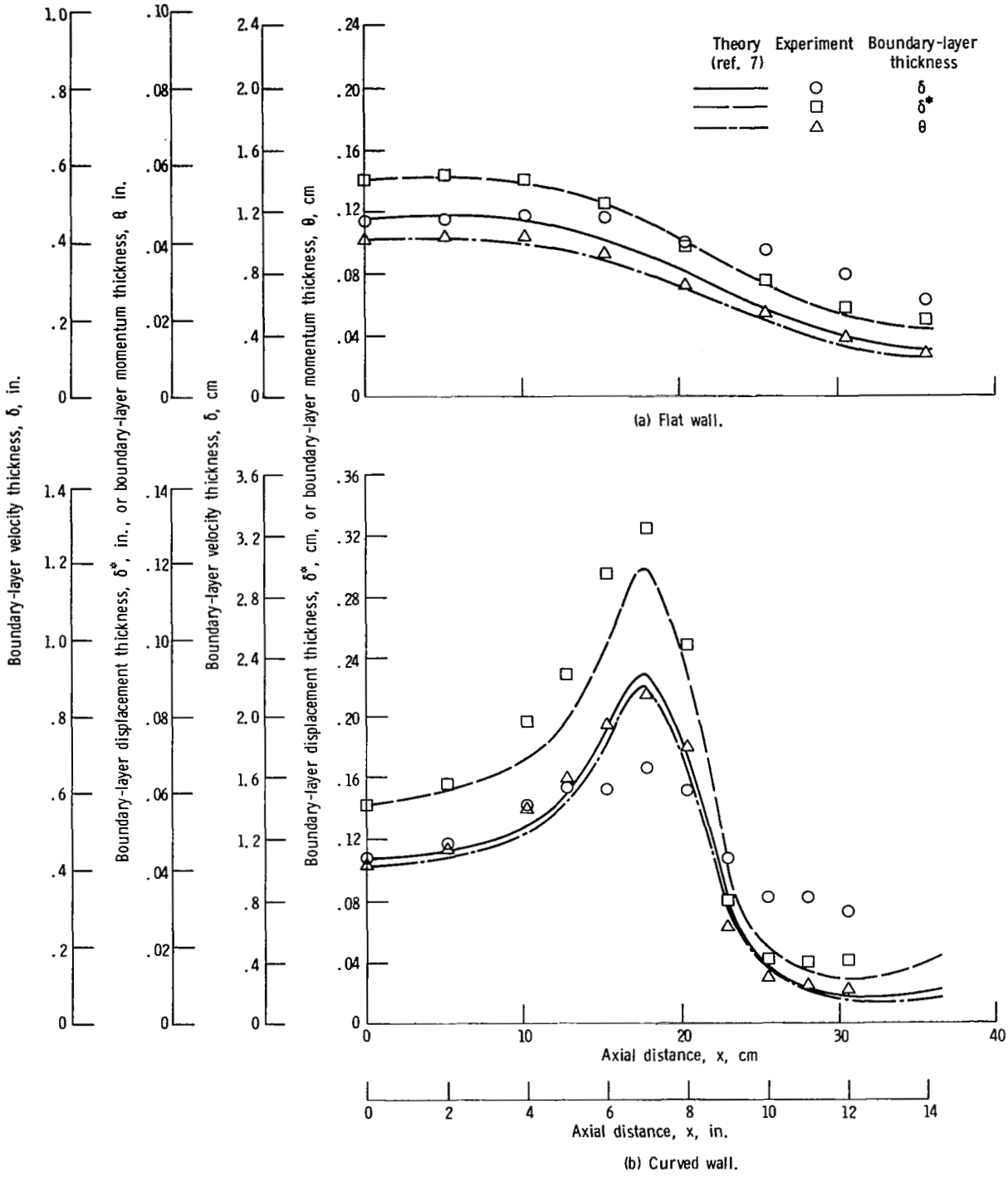

Figure 13. - Comparison of experimental and theoretical integral boundary-layer thicknesses.

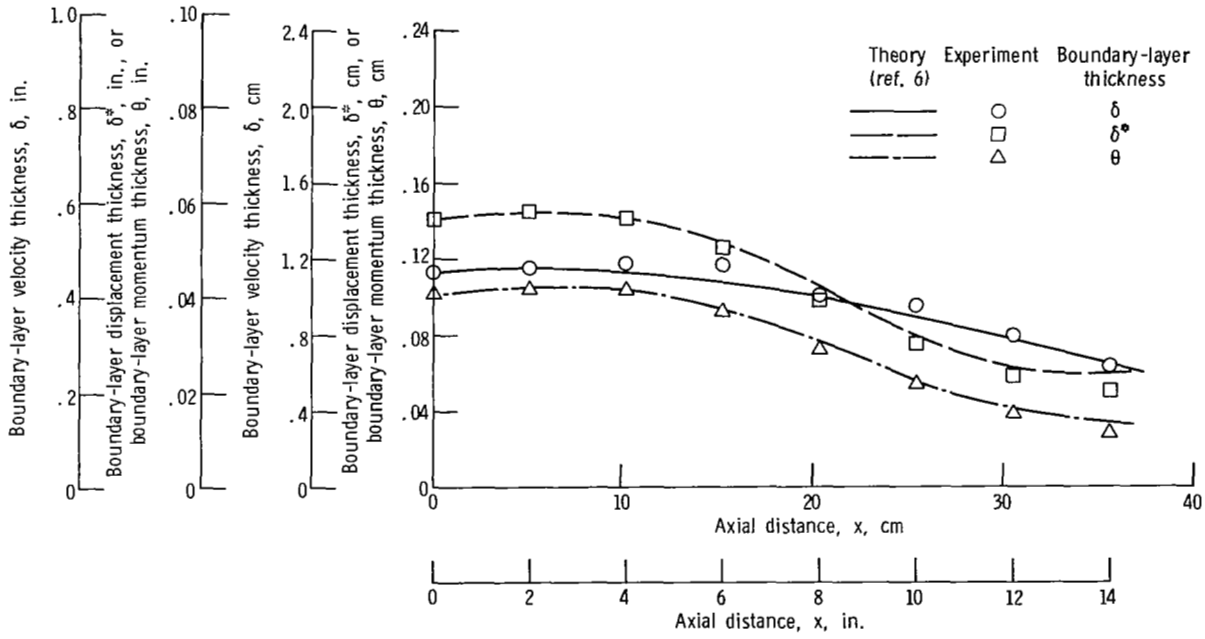

Figure 14. - Comparison of experimental and theoretical differential boundary-layer thicknesses on flat wall.

NASA-Langley, 1971 — 12 E-6496